Journal of Biomedical Optics 19(12), 126012 (December 2014)

Photoacoustic imaging using acoustic reflectors to enhance planar arrays

Robert Ellwood,* Edward Zhang, Paul Beard, and Ben Cox
University College London, Department of Medical Physics and Biomedical Engineering, Gower Street, London, WC1E 6BT, United Kingdom

Abstract. Planar sensor arrays have advantages when used for photoacoustic imaging: they do not require the imaging target to be enclosed, and they are easier to manufacture than curved arrays. However, planar arrays have a limited view of the acoustic field due to their finite size; therefore, not all of the acoustic waves emitted from a photoacoustic source can be recorded. This loss of data results in artifacts in the reconstructed photoacoustic image. A detection array configuration which combines a planar Fabry–Pérot sensor with perpendicular acoustic reflectors is described and experimentally implemented. This retains the detection advantages of the planar sensor while increasing the effective detection aperture in order to improve the reconstructed photoacoustic image. [DOI: 10.1117/1.JBO.19.12.126012]

Keywords: photoacoustic imaging; limited aperture; reflectors; image reconstruction; Fabry–Perot ultrasound sensors.

Paper 140575PR received Sep. 4, 2014; accepted for publication Nov. 19, 2014; published online Dec. 23, 2014.

1 Introduction

Planar sensor arrays used for photoacoustic (PA) imaging, e.g., interferometric optical sensors,[1] or capacitive micromachined ultrasonic transducers,[2] are often easier to fabricate (and interrogate), than curved or spherical arrays. However, their planarity also leads to a disadvantage: with a finite-sized planar sensor array, it is not possible to exactly measure sufficient data to recover the image anywhere in the imaged region. In other words, there is no "visible region"[3] (see Fig. 1). This "limited aperture," "limited view," or "partial data" problem results in blurring and artifacts in the reconstructed image.

Several techniques have been investigated to overcome the limited aperture problem. One approach is to introduce additional edges into the initial pressure distribution so that they are "visible" to the sensor array. Gateau et al.[4] proposed to do this by using speckle illumination to give the fluence more structure, and Wang et al.,[5] by using focused ultrasound to increase the Grüneisen parameter within the focal region (as it is typically temperature dependent). To obtain the full image, both methods require numerous partial images to be measured, which make these techniques slow. The limitations of both procedures are related to the extent to which they can form sharp features within the initial pressure distribution. Frikel and Quinto[6,7] show that windowing the data (apodising) can ameliorate the presence of sharp image artifacts, but it does not help to recover the missing edges. A more general approach, which is not specific to this type of artifact, could be to frame the image reconstruction in such a way that additional information about the image (priors) can be directly incorporated. For example, a total-variation penalty term could be used to promote piecewise constant features in the image,[8] or vessel filtering[9] could be used to reduce artifacts, although there must be vessel-like structures present for this to work. This paper takes a different approach and examines the use of multiple acoustic reflectors to increase the effective aperture by redirecting the sound waves that would otherwise have missed it, onto the sensor array. This allows parts of the image to be recovered that would otherwise be invisible; for example, edges that are close to perpendicular to the sensor plane. Huang et al.[10] also used an acoustic reflector positioned at about a 45 deg angle to a linear sensor array to extend its effective aperture and assist with the recovery of boundaries perpendicular to the sensor. As the exact angle of the reflector was unknown, it was adjusted during the image reconstruction to maximize the sharpness of the image. The acceptance angle of their piezoelectric transducer limited the improvement achievable. Li et al.[11] extended this work by investigating the use of two reflectors, one at each end of the array and each making a 30 deg angle with it. A limitation of this technique is that the entire object being scanned has to fit in the volume between the reflectors and the sensor. Increasing the reflector angles so that they are perpendicular to the array allows part of an object to be imaged while the remainder stays outside the imaging region, this would be beneficial in breast or small animal imaging. Using numerical simulations, Cox et al.[12] demonstrated that this arrangement could be used to extend the sensor's effective aperture and gave a fast exact reconstruction algorithm for this case. This paper presents an experimental validation of this approach.

The layout of the paper is as follows. Section 2 describes the use of acoustic reflectors to increase the effective aperture of the sensor. In Sec. 3, numerical simulations of this technique are presented. An experimental configuration for implementing this technique based on an optically addressed planar Fabry–Pérot (FP) ultrasound sensor is introduced in Sec. 4 and the images obtained using this scheme are presented in Sec. 5. Finally, a discussion of the limitations and practical capabilities of using acoustic reflectors to extend the effective aperture of the sensor is presented in Sec. 6.

*Address all correspondence to: Robert Ellwood, E-mail: robert.ellwood@ucl.ac.uk

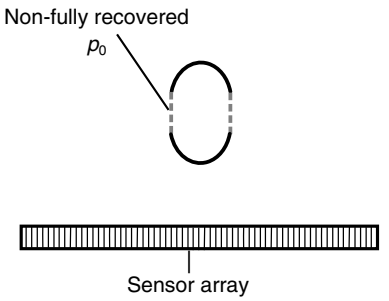

Fig. 1 The limited aperture, or partial data, problem. The limited aperture problem arises due to the finite size of the sensor. Waves traveling in some directions away from the photoacoustic (PA) sources are not detected by the sensor array, which means this sensor geometry has no "visible" region where the initial pressure distribution ($p0$) can be stably recovered. The visibility condition requires that for an edge in $p0$ to be recovered, the normal to this edge must pass through the array.

2 Theory: Reconstruction with Image Sources

Figure 2 illustrates the concept of using acoustic reflectors to extend the effective aperture of planar sensor arrays. An acoustically reflective cavity is formed by placing reflectors perpendicular to a planar sensor array. Acoustic waves emitted by the photoacoustic source are reflected from the reflectors and directed onto the sensor array. In this way, the wave fronts that would not have been directly detected by the detector array will be reflected onto the sensor. This arrangement of perpendicular reflectors has the advantage of not requiring the full enclosure of the sample under investigation, and it facilitates the use of a fast reconstruction algorithm.[12]

Various approaches could be used to reconstruct the initial pressure field from the data, including general approaches such as time reversal,[13] or model-based inversion.[14] Here, the fast image reconstruction algorithm proposed in Ref. 12 was used. It is based on the idea that having reflectors perpendicular to the sensor can be regarded as introducing image sources, thereby extending p_0 periodically with a period of twice the array width. The algorithm exploits this periodicity by matching the physical periodicity of the image sources with the periodicity inherent in the fast Fourier transform (FFT). In order to apply this technique, a mirrored copy of the recorded time series data is placed alongside the original time series data, and the reconstruction algorithm is applied to the combined dataset. In order to simplify the inverse problem, it is assumed that the acoustic reflectors are 100% reflective (pressure reflection coefficient of 1).

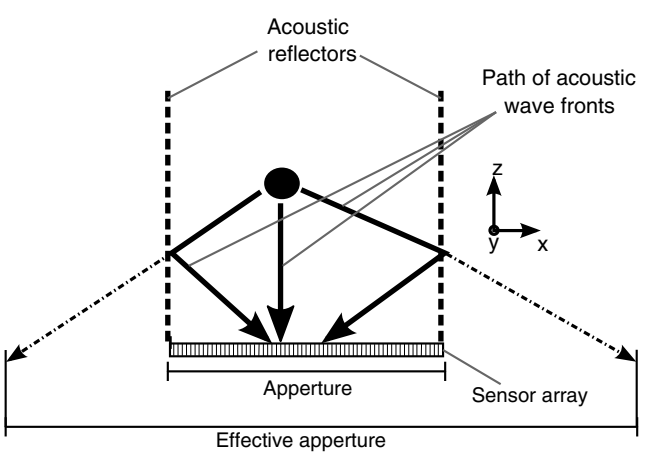

Fig. 2 Diagram demonstrating the technique developed to extend the effective aperture of a planar sensor array by using acoustic reflectors that are perpendicular to the sensor surface. Here, a side view of the reflector geometry with arrows indicating the effective extension in the aperture due to the reflection is shown. (The effective aperture size will, in general, be different for different points in the image.).

3 Numerical Simulations

Two separate groups of simulations were conducted to investigate the increase in the effective aperture with the presence of reflectors. The first group of simulations demonstrated the qualitative improvements in the image, the second group investigated the quantitative improvement in the reconstructed images as the acquisition time (and, therefore, the number of reflections acquired) increased.

3.1 *Simulation Investigating Qualitative Improvement in Two-Dimensional Knotted Phantom*

Two two-dimensional (2-D) simulations were conducted to investigate the increase in the effective aperture that could be gained using perpendicular reflectors. In one simulation, there were no reflectors (free-space propagation); in the other, reflectors were present. The simulations consisted of modeling the acoustic wave propagation and detection by a sensor array using a *k*-space pseudospectral time-domain acoustic propagation model, *k*-Wave.[15,16] In the first simulation, where no reflectors were present, absorbing boundary conditions were applied to all sides of the computational domain, simulating free-space propagation. For the second simulation, the reflections were simulated by first mirroring the domain about its right-hand edge (Fig. 3), and then setting the acoustic model to have periodic boundary conditions on the vertical sides, so that pressure waves leaving the domain at one wall will reappear at the other wall across the domain. Data were only acquired from the half of the computational domain representing real, as opposed to reflected, space. Absorbing boundary conditions were applied to the top and bottom edges of the domain. The initial pressure distributions were reconstructed from the simulated datasets using an FFT-based reconstruction algorithm.[12,17] Both simulations used an initial pressure distribution that was a 2-D representation of the knotted tube phantom experimentally used (Sec. 4) in order to facilitate qualitative comparison with the experimental results.

For both simulations, zero-mean random Gaussian noise was added to give a signal-to-noise ratio of 40 dB. A

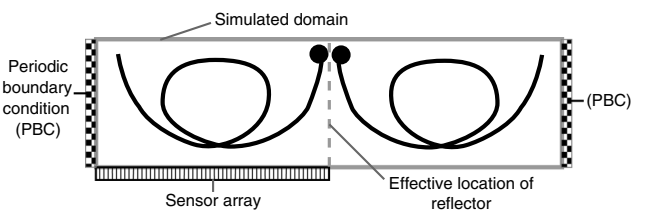

Fig. 3 Image of the numerical phantom used to simulate the acoustic field when reflections are present. Note the mirrored copy on the right-hand side (the circles at the tip of the phantoms are not present in the simulation and are shown here to illustrate the mirroring).

frequency-dependent absorption coefficient, $\alpha = a\omega^2$, was used, with $a = 2.17 \times 10^{-3}$ dB MHz^{-2} cm^{-1}, to simulate propagation in distilled water,[18] matching the experimental conditions investigated later. The acoustic field at the sensor array was recorded for 380 μs, which ensured that the majority of the acoustic energy had left the domain by the end of the simulation. (In the simulation where reflectors are present, the ratio of the sum of the acoustic pressure initially squared across the domain to that at the end of the simulation was 1.45×10^{-5}). The grid size for the free-space simulation was 129×129 with a step size of 100 μm, supporting spatial frequencies up to 7.34 MHz, with a temporal step size of 19.9 ns. The reverberant simulation had a grid size of 258×129 with a step size of 100 μm. The nonabsorbing sound speed and density for both simulations was 1482 ms^{-1} and 1000 kgm^{-3}, respectively, to simulate the phantom being in de-ionized water at 20°C.[18]

The simulated time series over the first 60 μs (a) without reflectors and (b) with reflections can be seen in Fig. 4; the reflections are clearly visible. Figure 5 shows (a) the true initial pressure distribution, (b) the image reconstructed without reflections present, and (c) the image reconstructed with reflections present. Clearly, there is an improvement in the image that includes the reflections; more of the features are visible in the image, and there are fewer artifacts. Most notably, the visibility of features that are tending toward being perpendicular to the sensor is considerably improved when reflections are used in the reconstructions.

3.2 *Improvement in Reconstruction with Number of Reflections*

To investigate the relationship between the improvement in the reconstructed image and the number of reflections recorded, a number of simulations were conducted using the same model and choices of parameters as above. In each simulation, an initial pressure distribution consisting of a single disk was simulated. These were placed at different locations within the domain to investigate the spatial dependence of the improvement in reconstruction (see Fig. 6). Each simulation was run for a total of 247 μs, which is a sufficient time for an acoustic wave to traverse the domain 20 times (20 × diagonal of domain/speed of sound within the domain), corresponding to a minimum of 20 reflections being recorded at the array for all spatial locations. For each source location, 20 reconstructions were performed, with the duration of the time series used in the reconstruction truncated between 5% and 100% of the total duration. By doing this, reconstructed

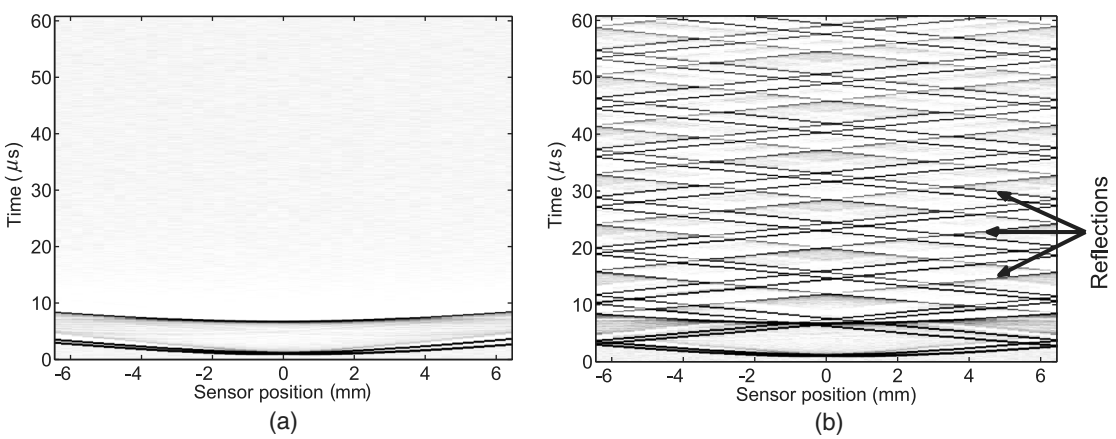

Fig. 4 The first 60 μs of the pressure time series from simulation, (a) with no reflectors present (b) with reflectors present. Time series were recorded up to 380 μs, but this first 60 μs only is shown here for clarity. The arrows draw attention to the presence of reflections in (b).

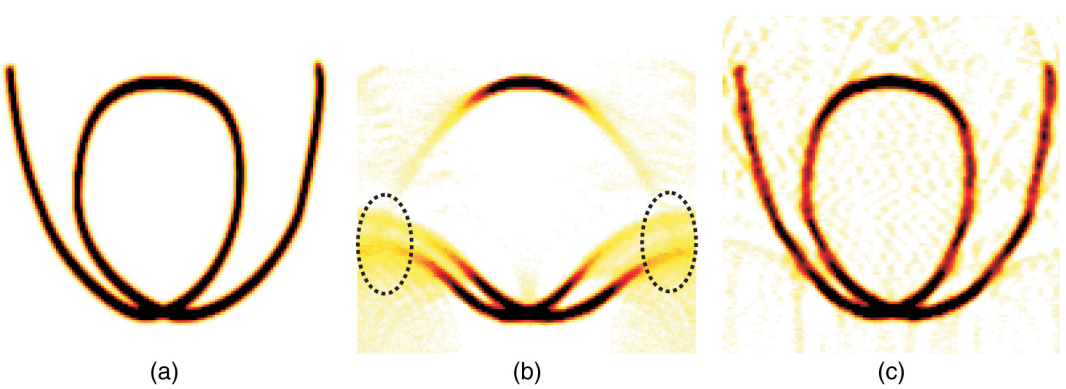

Fig. 5 (a) Initial pressure distribution, (b) reconstructions without reflections and (c) with reflections are shown. Note that including reflections improves visibility of features that are tending toward perpendicular relative to sensor. Artifacts are highlighted in (b) by dashed lines.

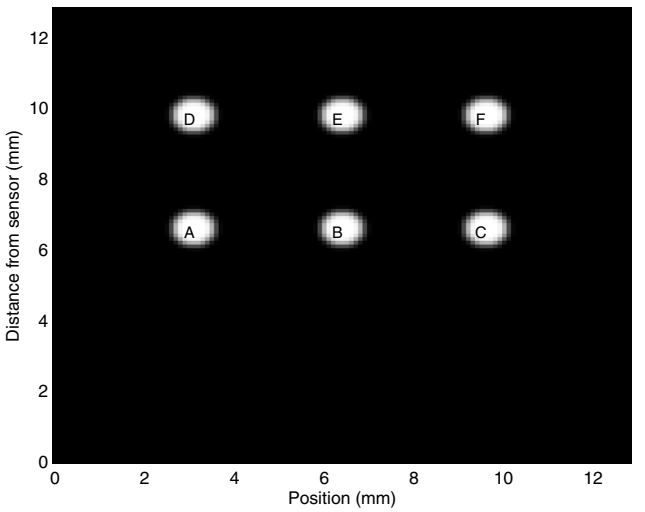

Fig. 6 Distribution of initial pressure sources used for each simulation. Each disk is labeled, (a–f).

images that incorporated different numbers of reflections were produced.

Each reconstructed image was compared to the initial pressure distribution by calculating the sum of the square difference (SSD) between them. This was normalized with respect to the SSD value for the first reconstruction where no reflections are present to give an error metric. In Fig. 7, the $\log_{10}$ of the error metric is plotted against the $\log_{10}$ of the duration of the time series (corresponding to the number of reflections) used in reconstruction. As the number of reflections included in the reconstruction increases, the error metric decreases, meaning that the reconstructions become closer to the initial pressure distribution, for all spatial locations. The error metric for reconstructions of disks closer to the sensor decreases more slowly with an increase in the number of reflections, as would be expected since more of the radiating acoustic wave is directly captured by the sensor. Minimal improvement in the reconstruction is achieved by collecting more than 10 reflections (Fig. 7 is plotted on a log scale). This is also expected, as the waves propagating in directions almost parallel to the detector will need to traverse the domain many times before reaching the detector array and both geometric spreading and absorption will reduce their amplitude, reducing the improvement in the reconstruction after a finite number of reflections.

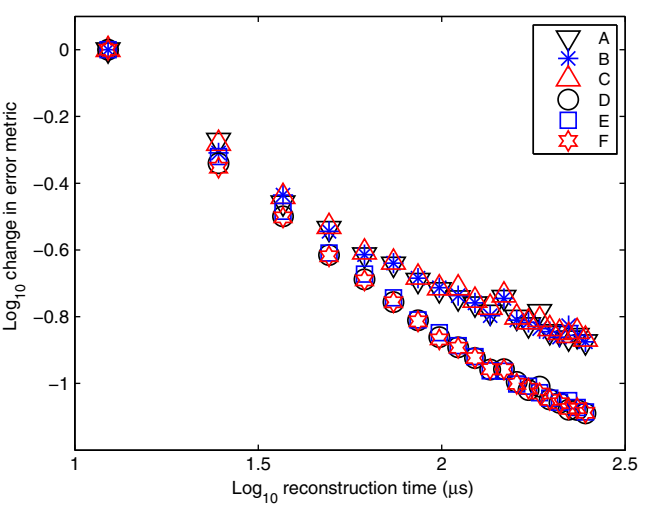

Fig. 7 Simulated results showing the proportional decrease (relative to the first reconstruction) in error metric [sum of square difference (SSD) between the reconstruction and initial pressure distribution ($p0$)], with an increase in length of reconstruction time, for initial pressure distributions at different locations. A minimum of one reflection occurs every time the acoustic wave traverses the domain (taking 12.3 μs), independent of the initial location of the source. Hence, the length of time used for the reconstruction determines the number of reflections included in the reconstruction. A, B, C, D, E, F corresponding to the locations seen in Fig. 6. The image improves more for positions further from the sensor.

4 Experimental Configuration

This section describes the experimental configuration used to investigate the use of perpendicular reflectors in extending the effective aperture of a sensor.

The acoustic reflectors consisted of four borosilicate crown (BK 7) glass prisms glued together to form a 1 cm^3 hollow cube faced with glass reflectors on the four vertical sides. This reflector arrangement was directly placed on the sensor surface. Prisms were chosen to reduce the effect of secondary acoustic reflections from the exterior wall of the glass re-transmitting into the water, being recorded, and corrupting the image. Glass being optically transparent had the advantage that it allowed the direct illumination of the region of interest; using opaque reflectors makes it difficult to achieve an even distribution of light inside the cavity. A minor limitation of using glass is that it is not perfectly acoustically reflecting; based on a sound speed and density of 5660 ms^{-1} and 2500 kgm^{-3} for glass, 1482 ms^{-1} and 1000 kgm^{-3} for water,[19] the pressure reflection coefficient for waves at a normal incidence to the boundary is $R = 0.81$. The reconstruction and simulation described in Secs. 2 and 3 assumed that the walls are 100% reflective, $R = 1$. This is further discussed in Sec. 6.

The acoustic sensor consisted of a 20-μm thick FP polymer film sensor with a −3 dB bandwidth of approximately 40 MHz.[1] The FP is addressed by a focused beam that is scanned from point to point across the sensor surface to synthesize a planar array. Using an acoustic sensor based on the FP allows the array to have a small element size without a decrease in the sensitivity. Elements with a smaller size more closely approximate the assumption in the reconstruction of omnidirectionality, which is beneficial when using acoustic reflectors due to the high angles of the later reflected waves. The acoustic reflector was directly placed on top of the sensor. The photoacoustic signal was generated using a fiber coupled Q-Switched Nd:YAG laser with a pulse duration of 10 ns that was backward mode coupled into the system as shown in Fig. 8.

Two phantoms were imaged with the acoustic reflectors present. The first phantom consisted of a tube (microbore extension line, MX590, Smiths Medical) that was knotted [see Fig. 9(a)]. The loop that this formed had both edges that are directly detectable by the sensor (with angles that are close to parallel to the sensor) and edges that would not be (with angles that are close to perpendicular to the sensor). This choice of phantom was made in order to demonstrate that including reflections will allow more of the edges to be reconstructed, corresponding to an effectively larger sensor aperture. The tube was filled with India ink diluted to 1% concentration so that the illuminating light can penetrate throughout

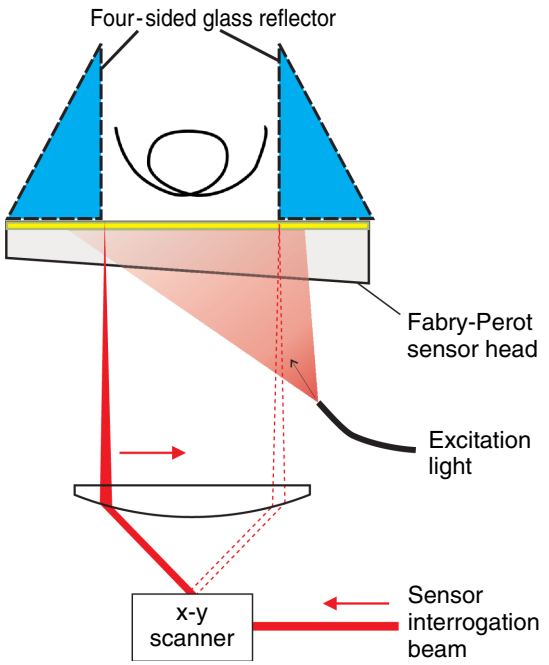

Fig. 8 Diagram of experimental imaging set-up showing the phantom and acoustic reflector arrangement.

the diameter of the tube and not be solely absorbed at the surface of the ink.

The second phantom consisted of a polymer ribbon, ~0.6 mm wide and 100-μm thick. This was twisted several times and held in place by gluing it between two acrylic armatures of a custom mount [see Fig. 9(b)]. The twisted plane nature of the phantom means that along the phantom's length its angle relative to the sensor changes. By imaging this phantom, the maximum angle of the side of the phantom relative to the sensor that can be reconstructed is found; from this the effective aperture of the sensor could be determined.

The chosen phantom was placed inside the acoustically reflecting cavity, which was placed on top of the FP sensor and filled with deionized water. A scan area of 11×12 mm was selected, which deliberately overlapped the walls, so that the exact position of the walls could be obtained from the measured data. In this way, the region of interest was defined, and measurements from outside this region were discarded prereconstruction. A step size of 100 μm was chosen as a compromise between a high spatial sampling and a dataset of easily manageable size. All wave components with frequencies below 7.5 MHz were spatially sampled at least two points per wavelength, which although below the 40 MHz bandwidth of the sensor, are not significantly lower than the highest frequencies expected in the signal. By inspecting the time series, it was found that the last reflections that were above the noise floor were observed at 22.6 μs; this defined the length of each acquired time series and thus the length of data used in the reconstruction.

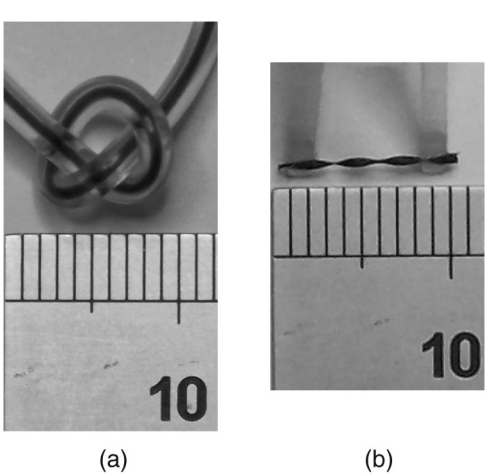

Fig. 9 Photo of the tube phantom (a) and twisted ribbon phantom mounted on custom acrylic mount (b) experimentally used. Scale in mm.

5 Experimental Results

5.1 *Time Series Data*

Figure 10 shows the time series recorded following the illumination of the twist phantom. Reflections from the side walls of the reflector can be seen in the time series just as in the simulation (indicated by the arrows in Fig. 10).

5.2 *Tube Phantom*

To investigate the influence of a few reflections compared to many on the reconstructions, two reconstructions were produced corresponding to a short measurement time (very few reflections) and a longer measurement time (several reflections). To replicate the case where only a few reflections are present, data after $t_{max} = 6.8$ μs was removed, the dataset was then zero padded and the transition between the data and the zeroes was smoothed using a Blackman window on the time series. This means that some reflections were still present but it approximated to the case without reflecting walls. In the second reconstruction, all of the data were used. Both cases are exactly reconstructed in the same way using the algorithm described in Sec. 5.

In Fig. 11, maximum intensity projections (MIPs) of the reconstructions for both cases can be seen, rendered in

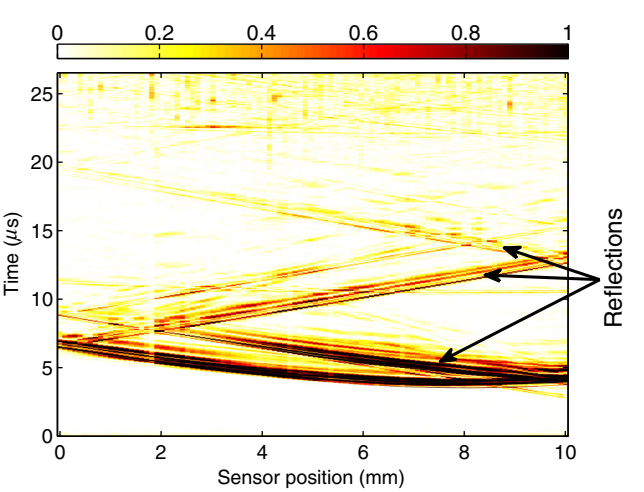

Fig. 10 Normalized pressure time series experimentally measured using the phantom shown in Fig. 9(b). Note that the reflections can be seen as a series of waves crossing the sensor surface, highlighted with arrows.

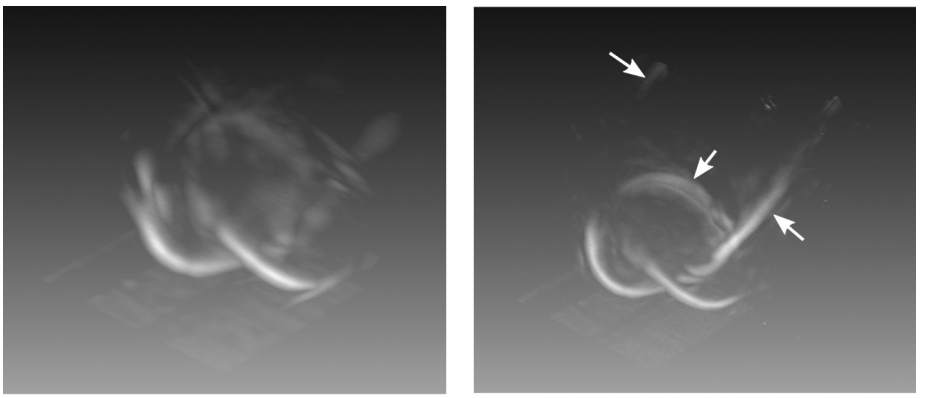

Fig. 11 Reconstructed initial pressure distribution displayed using Amira. (a) With only a few reflections (t max = 6.8 μs). (b) With all reflections (t max = 22.6 μs). Arrows in (b) highlight regions of improvement in reconstruction using more reflections. Note that the tube on the left-hand side of (b) is at a higher angle relative to the sensor and hence is not reconstructed.

Amira[20] (FEI Visualization Sciences Group). In the case where the data are reconstructed with all of the reflections present, it can be seen that the rear loop of the tube and part of the tube at a steep angle from the sensor are visible. In the case where fewer reflections are present, these features are not clearly defined and there are more artifacts.

A 2-D MIP of the image of the loop in side profile was used to give an estimate of how much the additional reflections increase the effective aperture. Lines connecting the last well-reconstructed points on each side of the loop image were extended until they crossed the plane of the sensor array. The effective aperture was then defined as the distance between the intersections with this plane (see Fig. 12). The case where only some of the reflections are present gives an effective aperture of 27.8 mm, whereas the case where all the reflections are present gives an effective aperture of 39.1 mm. This represents an increase in the linear aperture of ~40%. For a square-based cavity, both linear directions will see the same increase. This demonstrates an increase in the effective area of almost 100%.

5.3 *Twisted Ribbon Phantom*

The ribbon was positioned so that its length ran parallel to the sensor array in one axis. Images of the twisted ribbon phantom were reconstructed using short and long duration time series, as with the tube phantom [see Figs. 13(a) and 13(b), respectively]. In both cases, not all of the ribbon is recovered: the acoustic waves emanating from parts of the absorber that are perpendicular to the sensor array are not recorded, therefore, those edges do not appear in the images. In the case where fewer reflections are present, it can be seen that less of the ribbon is reconstructed. The reconstruction that uses fewer reflections is better on one side as the ribbon was placed close to one of the walls which resulted in the acoustic waves emitted by the portion of the ribbon tending toward the wall not being directly received.

The improvement in reconstruction with the presence of reflections is also seen when the reconstruction is stepped through as a series of slices along the length of the ribbon (see Fig. 14). In the case where all the reflections are present, the ribbons sides are recovered at angles closer to perpendicular

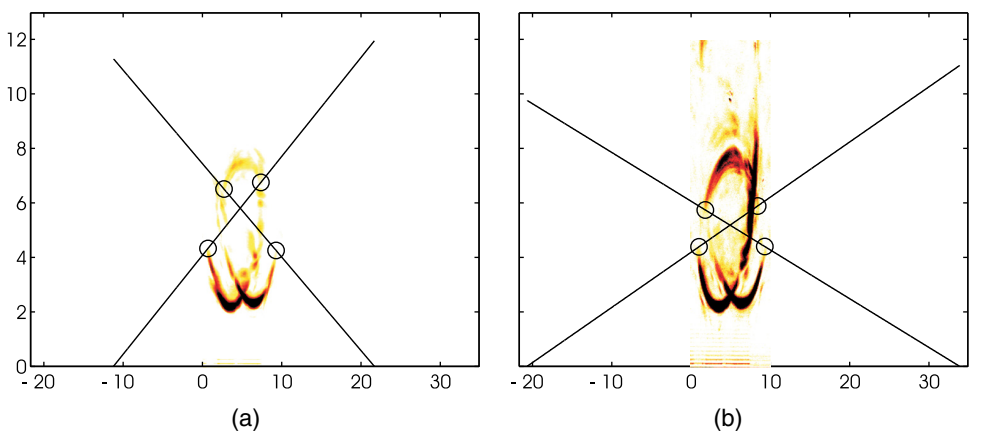

Fig. 12 Maximum intensity projection (MIP) of reconstructed initial pressure distribution (a) with fewer reflections (t max = 6.8 μs)—aperture length of 27.8 mm. (b) With all reflections (t max = 22.6 μs)—aperture length of 39.1 mm. Both images are produced with the same color scale. Black circles denote the last well-reconstructed point that was found. The lines are extrapolated from these points, where these lines reach zero (the location of the sensor) denotes the aperture length in this dimension.

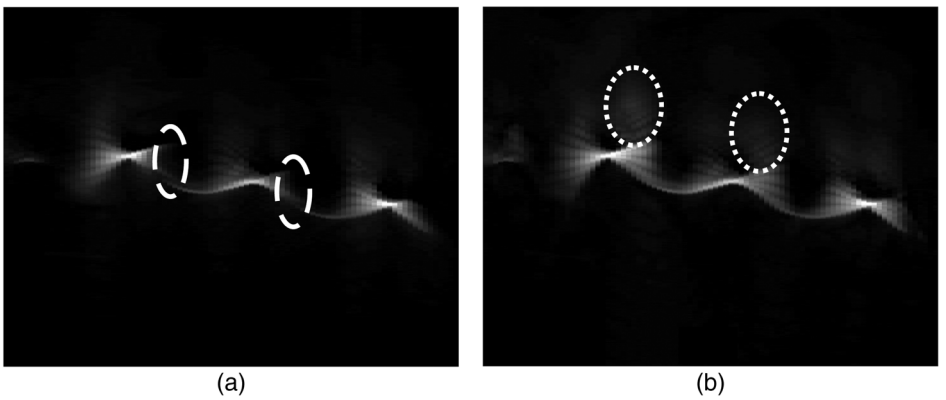

Fig. 13 Maximum intensity projection through side of the twisted ribbon for case with few reflections (a) and all reflections (b). Note that the asymmetry in the reconstruction for the case with fewer reflections where parts of the ribbon are not recovered (dashed white ovals). The reconstruction using all of the reflections still has limited view artifacts, emphasized by the dotted lines in (b), as wave fronts traveling close to parallel are not detected as they are below the noise floor of the detector when they reach the sensor due to spherical spreading and attenuation.

to the sensor than in the case where fewer reflections are present. This is seen in Fig. 14 by the ribbon being clearly visible in the fourth slice down in column c but not in column b.

The increase in the effective aperture length with more reflections is determined from the maximum recoverable angle of the ribbon to the sensor in the reconstruction. The maximum angle of the ribbon relative to the sensor that is stably reconstructed was found by stepping through the reconstruction a slice at a time until the ribbon was no longer visible. The slice before this corresponds to the last stably reconstructed edge of the phantom. The effective aperture was determined from this slice by thresholding the image and then applying a Hough transform.[21] The Hough transform detects the straight line formed by the ribbon in the reconstruction slice and outputs its position and angle. Using this position and angle information, a line perpendicular to the ribbon was extrapolated from the center of the ribbon (see Fig. 15). Where this extrapolated line met the sensor plane was determined to be the effective aperture, which in this case was 14.3 mm. This represents a 43% increase in the aperture length.

6 Discussion

Due to the nature of acoustic propagation, the ultrasonic pulses emitted by the photoacoustic source will propagate in all directions. While the reflectors help in collecting more of this field than would have otherwise been collected, those parts traveling parallel or close to parallel to the sensor will not reach the sensor for a long time. Furthermore,

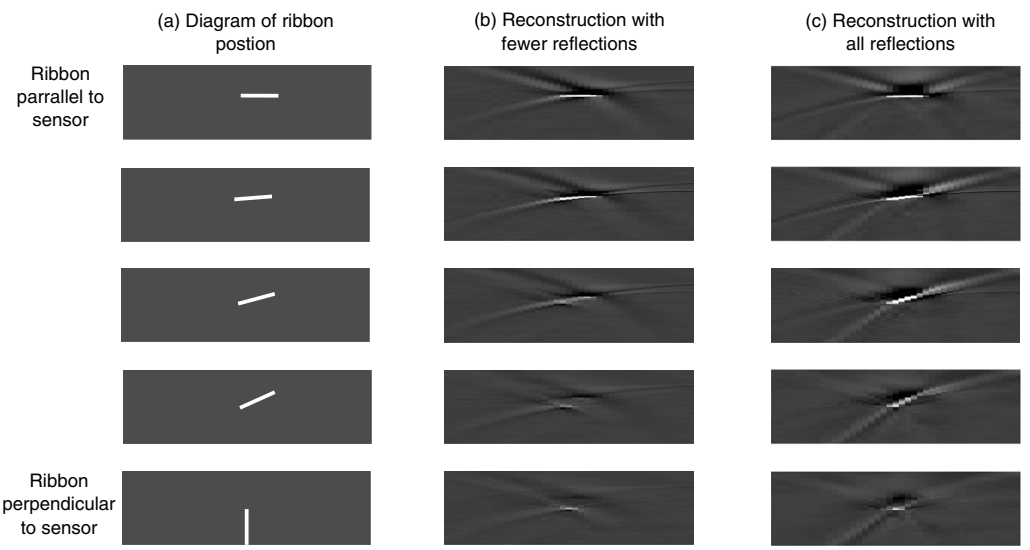

Fig. 14 Series of slices stepping along the length of the reconstruction of the twisted ribbon for case with few reflections (b) and all reflections (c). Column (a) shows a diagrammatic representation of the ribbons position. Each slice corresponds to the ribbon being at a different angle to the sensor from parallel at the top to perpendicular at the bottom. As the ribbon moves from being parallel to perpendicular, it quickly disappears from the reconstruction with fewer reflections, while the ribbon is visible in the reconstruction with all the reflections present until it becomes close to perpendicular to the sensor.

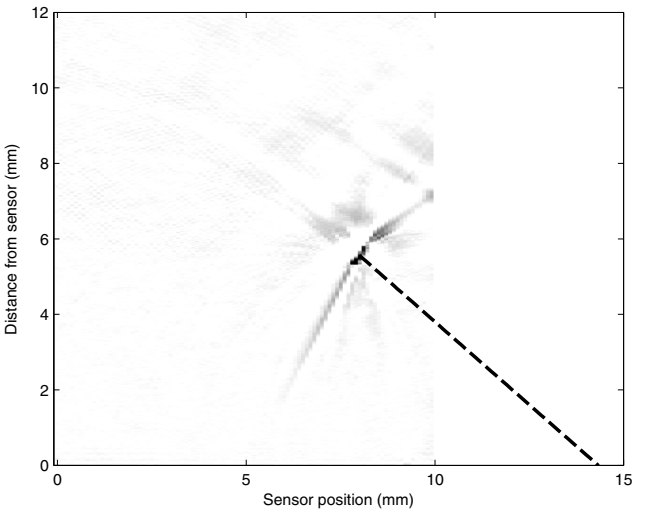

Fig. 15 Reconstruction of ribbon at the steepest angle that was fully recoverable. Dashed line runs perpendicular to the ribbon, denoting the maximum aperture.

because of the geometrical spreading (and absorption) that the waves undergo, the later arrivals will be significantly reduced in amplitude. (Some of the effects of attenuation could be compensated for using time variant filtering,[22] though care must be taken to ensure high frequency noise components are not excessively amplified.) The proportion of the total pressure field that is collected will, therefore, be ultimately limited by the finite noise floor of the detector and not the finite size of the sensor array. This reflector and sensor configuration, while offering an improvement over a planar sensor, still does not have a region where the initial pressure field is fully recoverable; there is still no "visible" region; however, it does represent an improvement.

As well as attenuation due to absorption and spreading, the loss at the reflectors should be considered. The image reconstruction algorithm was based on the assumption that the reflectors had a pressure reflection coefficient of 1, i.e., they are 100% reflective. In practice, waves normally incident to reflectors will experience a reflection coefficient $R < 1$. Silicon and tungsten carbide have high acoustic impedances and reflection coefficients of 0.92 (velocity of 11820 ms^{-1} and density of 3160 kgm^{-3} [23]) and 0.97 (velocity of 6655 ms^{-1} and density of 15,000 kgm^{-3} [19]), respectively, but are optically opaque which complicates the illumination of the sample. A water-air boundary has a pressure reflection coefficient of -1, and the reconstruction algorithm could be adapted to this case, but in implementing such a boundary it would be necessary to use a membrane to contain the water, and the water-membrane-air boundary only exhibits this ideal behavior over a narrow range of frequencies.[24] As PA is inherently broadband, this is a drawback. In these experiments, borosilicate glass was used: it has quite a large acoustic impedance ($R = 0.81$) and it is optically transparent, which allows the sample to be illuminated from all sides. At incident angles above 25.6 deg relative to the normal of the reflecting boundary, the waves will undergo total internal reflection, matching the $|R| = 1$ assumption of the perfect reflecting boundary used in the reconstruction. However, these waves will undergo a phase change on reflection, so their contributions to the final reconstructed image will be blurred to some extent. For the majority of reflected waves with incident angles greater than 25.6 deg relative to the normal to the boundary, the phase shift in the reflected wave is ~340 deg. As this phase shift remains relatively constant for a range of reflection angles, it may be possible to compensate for it in later arrivals by introducing a virtual boundary offset in the positions of the walls used in the reconstruction by a distance equivalent to the phase shift.[25] This is not implemented on the results presented here, but is left as future work.

Waves traveling at steeper angles will arrive at later times and will, therefore, either be significantly attenuated or not detected at all.

A further assumption implicit in the image reconstruction was that the reflectors were perpendicular to the sensor array. In these experiments, the uncertainty in the perpendicularity of the walls was estimated using digital calipers to be approximately 1 deg. This will affect the acoustic path of the reflected waves and the location of their contributions to the final reconstruction. This is demonstrated in Fig. 16 for two reflections. An initial pressure source p_0 is reflected in wall A which is at a slight angle (ε) to vertical, producing a reconstruction in position 1 (which would be subsequently introduced into the true domains reconstruction). When the first reflection is subsequently reflected at wall B this produces a reconstruction at position 2. The subsequent reflections' contribution to the reconstruction become erroneously placed further away.

The erroneous placement of the contribution to the reconstructed pressure field $(x_m^{\mathrm{error}}, y_m^{\mathrm{error}})$ following the m'th reflection due to the wall being at an angle (ε) away from perpendicular can be described by the following equation for an even number of reflections (assuming the first reflection occurs from the tilted wall):

$$\begin{bmatrix} x_m^{\mathrm{error}} \\ y_m^{\mathrm{error}} \end{bmatrix} = \left\{ (R_0 R_\varepsilon)^{m/2} \begin{bmatrix} x_0 \\ y_0 \end{bmatrix} + \sum_{i=0}^{(m/2)-1} (R_0 R_\varepsilon)^i \begin{bmatrix} 2d \\ 0 \end{bmatrix} \right\} \mathrm{mod}_x(2d), \quad (1)$$

where R_0 and R_ε are the reflection matrices for the walls when they are normal and angled by ε away from normal toward the sensor defined as

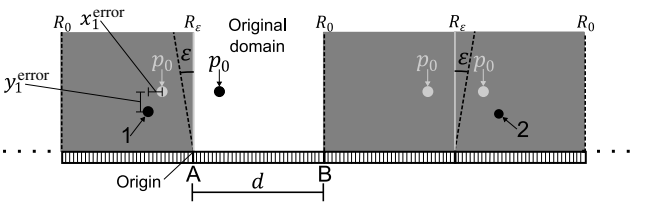

Fig. 16 Diagram depicting the propagation of misplacement of reconstructions of the initial pressure source ($p0$) caused by an error in the angle of a wall (ε), for the first two reflections. The diagram shows the placement of the reconstructed field due to a reflection at wall A to be at point 1. The subsequent reflection at wall B produces the reconstruction at point 2. Due to the symmetry of this technique, these misplaced reconstructions from each reflection will also occur in the original sensors domain. Also shown are the virtual domains (gray shaded area either side of original domain).

$$R_0 = \begin{bmatrix} -1 & 0 \\ 0 & 1 \end{bmatrix},$$
$$R_\varepsilon = \begin{bmatrix} \sin^2\varepsilon - \cos^2\varepsilon & 2\sin\varepsilon\cos\varepsilon \\ 2\sin\varepsilon\cos\varepsilon & \cos^2\varepsilon - \sin^2\varepsilon \end{bmatrix}. \quad (2)$$

The $\mathrm{mod}_x(2d)$ in Eq. (1) indicates that the modulo operation applies only to the x component, i.e., it restricts the reconstructed image sources to the region $0 \le x < 2d$. However, the final reconstructed image must lie between the reflectors, in the region $0 \le x \le d$; therefore, those reconstructed sources for which $x_{\mathrm{error}} > d$ must subsequently be folded back into the image region:

$$\begin{bmatrix} x_m^{\mathrm{error}} \\ y_m^{\mathrm{error}} \end{bmatrix} = R_0\left(\begin{bmatrix} x_m^{\mathrm{error}} \\ y_m^{\mathrm{error}} \end{bmatrix} - \begin{bmatrix} d \\ 0 \end{bmatrix}\right) + \begin{bmatrix} d \\ 0 \end{bmatrix}. \quad (3)$$

Using this analytical solution, the location of the contribution to the reconstruction from each reflection can be found, as shown in Fig. 17, for a wall with an angle of 1 deg away from perpendicular for the first 20 reflections. For the first two reflections, the contributions are within 300 μm of the placement of the initial p_0; this rises to 1 mm for four reflections and increases significantly after this. Evaluating the time series data from the experimental measurements, a maximum of three reflections are observed. The error in the placement of the contribution due to the reflections can be estimated as 300 μm. Because the spatial sampling size of the images produced is 100 μm, this represents a significant uncertainty. It is clear that the angle of the walls relative to the sensor is very important in terms of the gain in the effective aperture length. Using alternate manufacturing techniques, such as milling out the reflective cavity from a solid block of material, to construct the reflector could significantly reduce this error and improve the resolution of the final reconstruction.

It should be noted that this technique is resilient to the practical limitations discussed above and can be successfully implemented to extend the aperture of planar sensors.

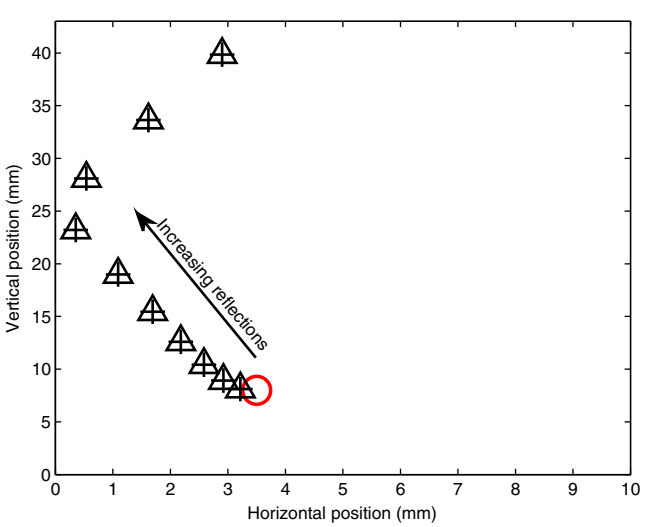

Fig. 17 Plot of the contributions to the reconstruction for the first 20 reflections where one wall is 1 deg away from perpendicular in a reflective cavity 10 mm long. The circle represents the initial location, the cross and triangles represent contributions from the odd and even reflections, respectively.

7 Conclusion

It has been experimentally demonstrated that using acoustic reflectors perpendicular to a planar sensor array can extend the effective detection aperture of the array, and thereby improve the quality of the photoacoustic images. Extending the effective aperture allows the sensor array to capture a larger solid angle of the emitted acoustic field, which in turn allows the recovery of features in the initial pressure distribution that are not visible to the planar sensor alone. The estimated increase in effective aperture is ~40% in each direction, which is an increase in the effective area of the sensor array by approximately 100%. While this is a significant improvement, full view reconstructions are still not possible using this technique, as extending the aperture does not create a "visible" region. Furthermore, the benefit of recording more and more reflections decreases due to the geometric spreading of the wavefield. In summary, using acoustic reflectors is a cost-effective and easily implementable way of increasing the effective detection aperture of a planar array, which can result in improved photoacoustic images.

Acknowledgments

This work was supported by Engineering and Physical Sciences Research Council (EPSRC) and European Union project FAMOS (FP7 ICT, Contract No. 317744).

References

1. E. Zhang, J. Laufer, and P. C. Beard, "Backward-mode multiwavelength photoacoustic scanner using a planar Fabry-Perot polymer film ultrasound sensor for high-resolution three-dimensional imaging of biological tissues," *Appl. Opt.* **47**(4), 561–577, (2008).
2. S. Vaithilingam et al., "Capacitive micromachined ultrasonic transducers (CMUTs) for photoacoustic imaging," *Proc. SPIE* **6086**, 608603 (2006).
3. Y. Xu et al., "Reconstruction in limited-view thermoacoustic tomography," *Med. Phys.* **31**(4), 724–33 (2004).
4. J. Gateau et al., "Improving visibility in photoacoustic imaging using dynamic speckle illuminiation," *Opt. Lett.* **38**(23), 5188–5191 (2013).
5. L. Wang et al., *Thermal Encoded Photoacoustic Tomography*, Photons Plus Ultrasound, SPIE Photonics West, San Fransisco (2014).
6. J. Frikel and E. T. Quinto, "Artifacts in incomplete data tomography—with applications to photoacoustic tomography and sonar," pp. 1–21, arXiv mathematics, arXiv:1407.3453 (2014).
7. J. Frikel and E. T. Quinto, "Characterization and reduction of artifacts in limited angle tomography," *Inverse Probl.* **29**(12), 125007 (2013).
8. L. Yao and H. Jiang, "Photoacoustic image reconstruction from few-detector and limited-angle data," *Biomed. Opt. Express* **2**(9), 2649–2654 (2011).
9. T. Orauganti, J. G. Laufer, and B. E. Treeby, "Vessel filtering of photoacoustic images," *Proc. SPIE* **8581**, 85811W (2013).
10. B. Huang et al., "Improving limited- view photoacoustic tomography with an acoustic reflector," *J. Biomed. Opt.* **18**(11), 110505 (2013).
11. G. Li et al., "Broadening the detection view of high-frequency linear-array-based photoacoustic computed tomography by using planar acoustic reflectors," *Proc. SPIE* **8943**, 89430H (2014).
12. B. T. Cox, S. R. Arridge, and P. C. Beard, "Photoacoustic tomography with a limited- aperture planar sensor and a reverberant cavity," *Inverse Probl.* **23**, 95–112 (2007).
13. B. E. Treeby, E. Z. Zhang, and B. T. Cox, "Photoacoustic tomography in absorbing acoustic media using time reversal," *Inverse Probl.* **26**, 115003 (2010).
14. C. Huang et al., "Full wave iterative image reconstruction in photoacoustic tomography with inhomogeneous media," *IEEE Trans. Med. Imaging* **32**(6), 1097–1110 (2013).
15. B. E. Treeby and B. T. Cox, "k-Wave: MATLAB toolbox for the simulation and reconstruction of photoacoustic wave fields," *J. Biomed. Opt.* **15**(2), 021314 (2010).

16. B. E. Treeby and B. T. Cox, "k-Wave MATLAB toolbox," 2013, http://www.k-wave.org/ (12 February 2014).
17. K. P. Köstli et al., "Temporal backward projection of optoacoustic pressure transients using Fourier transform methods," *Phys. Med. Biol.* **46**, 1863–1872 (2001).
18. T. L. Szabo, *Diagnostic Ultrasound Imaging: Inside Out*, 2nd ed., p. 785, Elsevier Academic Press, Oxford, Amsterdam, and San Diego (2014).
19. G. W. C. Kaye and T. H. Laby, *Tables of Physical and Chemical Constants*, p. 29,30,74,76, Longman, London, and New York (1986).
20. Visualization Sciences Group "Amira visualization software," 2013 http://www.vsg3d.com/amira/overview (12 February 2014).
21. R. O. Duda and P. E. Hart, "Use of the Hough transformation to detect lines and curves in pictures," *Commun. ACM* **15**(1), 11–15 (1972).
22. B. E. Treeby, "Acoustic attenuation compensation in photoacoustic tomography using time-variant filtering," *J. Biomed. Opt.* **18**(3), 036008 (2013).
23. R. G. Munro, "Material properties of a sintered α-SiC," *J. Phys. Chem. Ref. Data* **26**(5), 1195–1203 (1997).
24. Z. Yang et al., "Membrane-type acoustic metamaterial with negative dynamic mass," *Phys. Rev. Lett.* **101**(20), 204031 (2008).
25. Z. Yang and C. Tindle, "Complex effective depth of the ocean bottom," *J. Acoust. Soc. Am.* **93**(1), 205–213 (1993).

Biographies of the authors are not available.